Reprinted from **APPLIED OPTICS,** Vol. 14, page 984, April 1975

Reflective Optics System for Uniform Spherical Illumination

C. R. Phipps, Jr., S. E. Bodner, and J. W. Shearer

A reflective optical system is described that permits nearly uniform illumination of a small sphere with one or two laser beams. The primary application of this device is to studies of laser-driven implosion of small targets. Other applications include the production of plasma by optical breakdown of gases for spectroscopic studies and for optimum light collection in intensity-limited plasma diagnostics. Simple calculations show that the intensity mapping properties of this system are not excessively sensitive to variations in the radial intensity distribution nor to departures from diffraction-limited propagation in the input beams. Optical damage and the illuminated solid angle required at the focus determine the size of the device.

Introduction

Experimental programs are underway at several laboratories with the intent of initiating deuterium–tritium thermonuclear reactions in small pellets by means of a laser-driven implosion. An important prerequisite for achieving the required density and temperature is the ability to illuminate the fuel pellet from 4π sr with substantial synchronism and uniformity.

Published estimates of the necessary illumination uniformity range from 10% to 20%[1,2] depending on the models employed for thermal conduction, magnetic field diffusion, etc. Laser systems now being built for fusion experiments are designed to achieve the required optical energy in several beams.

Individual optics designed to focus several beams onto a spherical target are not simple, even when as many as twenty beams are involved. Also, tailoring of the overlap among beams must be done on a scale of tens of microns. Such tailoring would be easier if it could be accomplished prior to focusing, at the entrance pupil of a single optical system for pellet illumination.

Such an optical system should be reflective, for reasons of optical damage resistance, freedom from nonlinear refractive effects, and wavelength-invariance of focal properties.

In this paper, two designs are described for optical systems that satisfy the requirements outlined above. It is not the purpose of this paper to assess the problems involved in fabricating these systems. However, two optical fabricators have been contacted who claim that they can make such systems with adequate optical quality, and one of them has done so.

When this work was done, all authors were with Lawrence Livermore Laboratory, University of California, Livermore, California 94550; C. R. Phipps is now with Los Alamos Scientific Laboratory, Los Alamos, New Mexico 87544; S. E. Bodner is now with the U.S. Naval Research Laboratory, Washington, D.C. 20375
Received 6 May 1974.

One-Beam Illumination System

Figure 1 illustrates a conceptual system that has the desired intensity mapping properties for a single laser beam possessing rotational symmetry about the propagation axis.

An elliptical mirror of eccentricity e and semimajor axis a has the target pellet at one focus F_1. A convex parabolic mirror with semilatus rectum p shares the major axis and conjugate focus F_2 of the elliptic mirror. A cylindrically symmetric, collimated input beam has radial intensity profile $I_b(\rho)$ and shares the elliptic mirror major axis. Incident radiation is first reflected by the parabolic mirror, with a virtual focus at F_2, and then by the elliptic mirror, generating a real focus at F_1.

This system can provide 4π illumination at F_1, except in two shadow cones caused by deletion of the elliptic mirror surface at the primary mirror and entrance aperture locations. The degree of uniformity achieved in the intensity distribution at F_1 depends on the form of the input distribution $I_b(\rho)$ and waist size w, as well as the parameters p and ρ_{max}. The focus-and-directrix properties of the conic sections employed guarantee synchronism at F_1 if the input beam is properly aligned. The output distribution $I_1(1,\theta)$ is derived on a unit sphere centered at F_1, for convenience in scaling the solution to a specific target radius. We will derive the mapping function

$$f(\rho,\theta) = I_1(1,\theta)/I_b(\rho) \tag{1}$$

for this specific geometry. The calculation is done in the geometric optics limit and involves only the converging wavefront intensity. These approximations are valid for target radii much smaller than the input beam waist and appreciably larger than the incident light wavelength λ_0. The error involved is less than 1% for diffraction-limited input beams if the target radius lies in the range $0.07w \gtrsim r_T \gtrsim 2\lambda_0$. Diffraction effects are treated later in more detail.

Referring again to Fig. 1, the parabolic mirror surface is given by

$$R(\phi) = p \sec^2(\phi/2) \tag{2}$$

and that of the elliptic mirror by

$$r_1(\theta) = a(1 - e^2)/(1 - e \cos\theta). \tag{3}$$

From the properties of an ellipse,

$$r_1(\theta) + r_2(\phi) = 2a. \tag{4}$$

The angles ϕ and θ are uniquely related for $0 \leq \theta, \phi \leq \pi$ by

$$\cos\phi = |2e - (1 + e^2)\cos\theta|/|(1 + e^2) - 2e\cos\theta| \tag{5}$$

or

$$\sin\phi = (1 - e^2)\sin\theta/|(1 + e^2) - 2e\cos\theta|. \tag{6}$$

Differentiation of Eq. (6) shows that

$$d\phi/d\theta = -(\sin\phi/\sin\theta) = -|r_1(\theta)/r_2(\phi)| \tag{7}$$

from which

$$r_2(\phi)d\phi = -r_1(\theta)d\theta. \tag{8}$$

Also, it is easily shown that

$$R(\phi)d\phi = d\rho. \tag{9}$$

Equations (8) and (9) are a consequence of the physical fact that the cross section of a differential pencil of rays is unchanged by reflection at a continuous surface. In the devices considered in this paper, the optic surfaces are conic sections arranged so as to guarantee that all wavefronts are spheres in the geometric optics limit. Therefore, the inverse-square law[3,4] applies, and the desired mapping function onto the unit sphere for the present system is given by

$$f(\rho, \theta) = (Rr_1/r_2)^2 \tag{10}$$

or

$$f(\rho, \theta) = p^2|(1 - e)/(1 + e)|^2 \csc^4(\theta/2). \tag{11}$$

The inverse mapping function will also be required. This function is given by

$$g(\rho, \phi) = I_b(\rho)/I_1(1, \theta) = (r_2/Rr_1)^2. \tag{12}$$

In terms of the parameters ϕ and ρ, this is

$$g(\rho, \phi) = I_b(\rho)/I_1(1, \theta) = (1/p^2)\{(1 - e^2)/|(1 + e^2) - 2e\cos\phi|\}^2 \cos^4(\phi/2).$$

In cylindrical coordinates, since $(\rho/2p) = \tan(\phi/2)$,

$$g(\rho/p) = (1/p^2)|(1 - e)/(1 + e)|^2/\{|(1 - e)/(1 + e)|^2 + (\rho/2p)^2\}^2. \tag{13}$$

In particular, if

$$e \longrightarrow \frac{1}{3}, g(\rho/p) \longrightarrow 4/p^2|1 + (\rho/p)^2|^2. \tag{13a}$$

This specialization is useful because attention will later be focused on situations where $e = 1/3$.

Equations (12) and (11) permit plotting $I_1(1,\theta)$ given an $I_b(\rho)$. Equation (13) is the input distribution that gives unit intensity for the converging wavefront at all points on the unit sphere at F_1 outside the shadow cones.

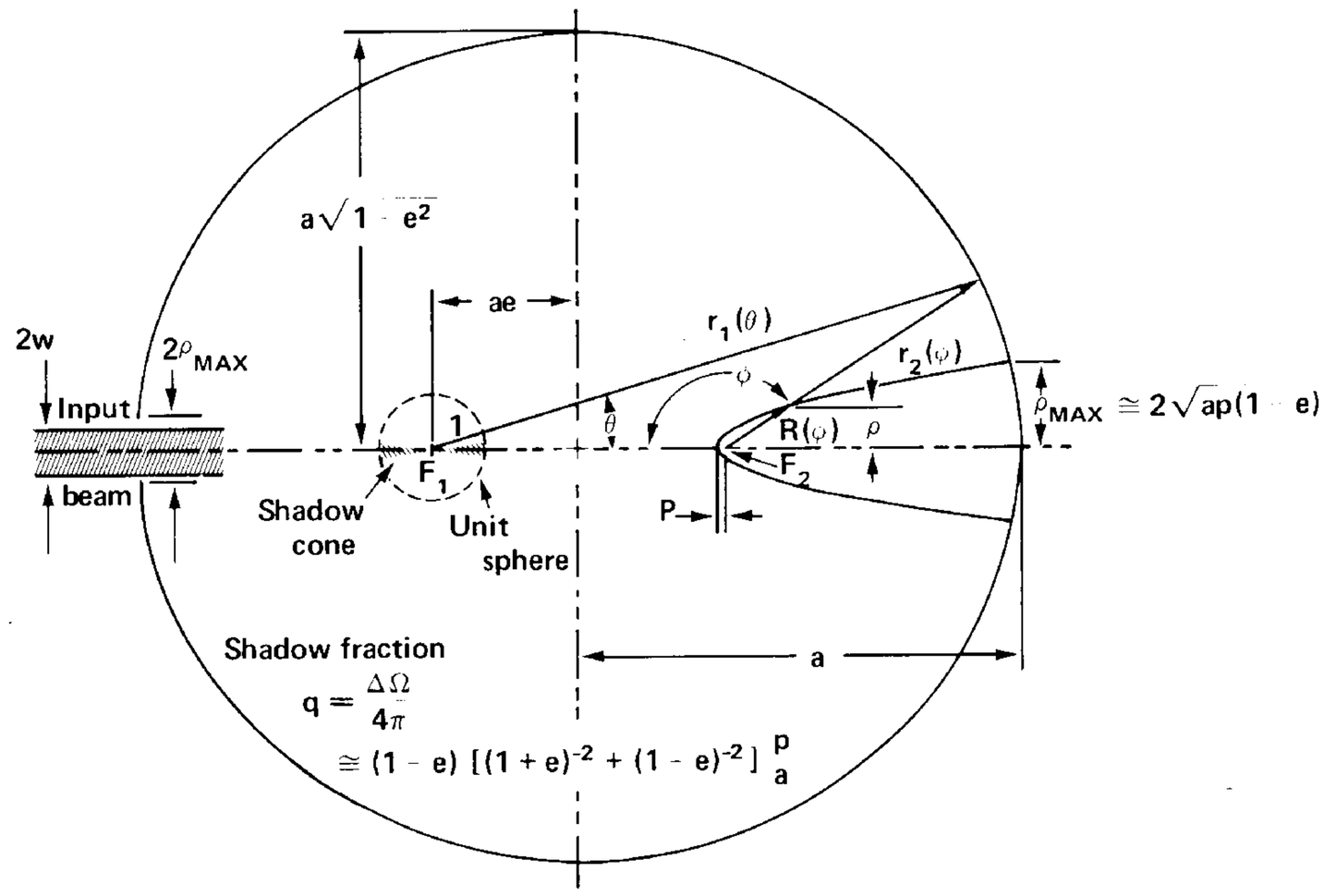

Fig. 1. One-beam illumination system with parabolic primary.

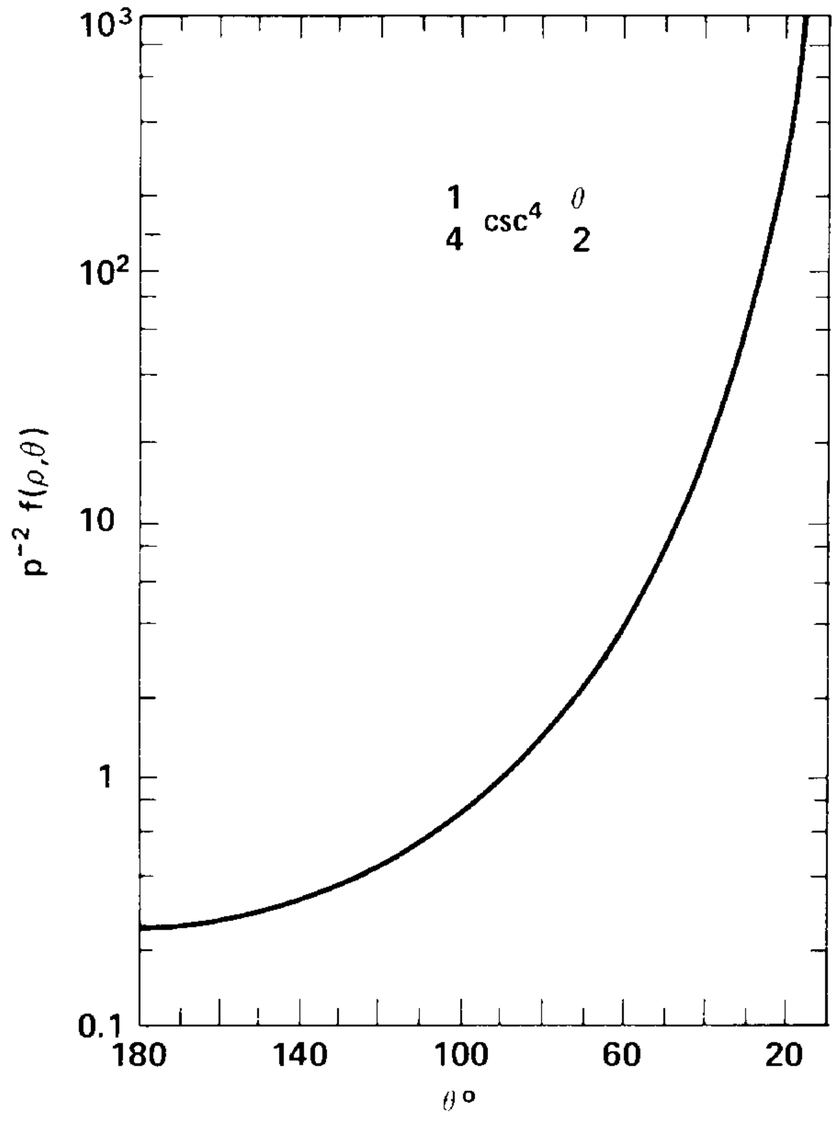

Fig. 2. $f(\rho,\theta)$ vs. θ for $e = 1/3$.

The intersection radius of the two mirror surfaces is

$$\rho_{\max} = 2\{ap(1 - e)\{1 - |p/a(1 + e)|\}\}^{1/2} \approx 2|ap(1 - e)|^{1/2}. \quad (14)$$

Setting the radius of the input pupil equal to $\rho_{\max}$, these cones have approximate total solid angle fraction given by

$$q = \Delta\Omega/4\pi \sim (1 - e)|(1 + e)^{-2} + (1 - e)^{-2}|(p/a). \quad (15)$$

For example, in Fig. 1 where $e = 1/3$, $q = 2.3\%$.

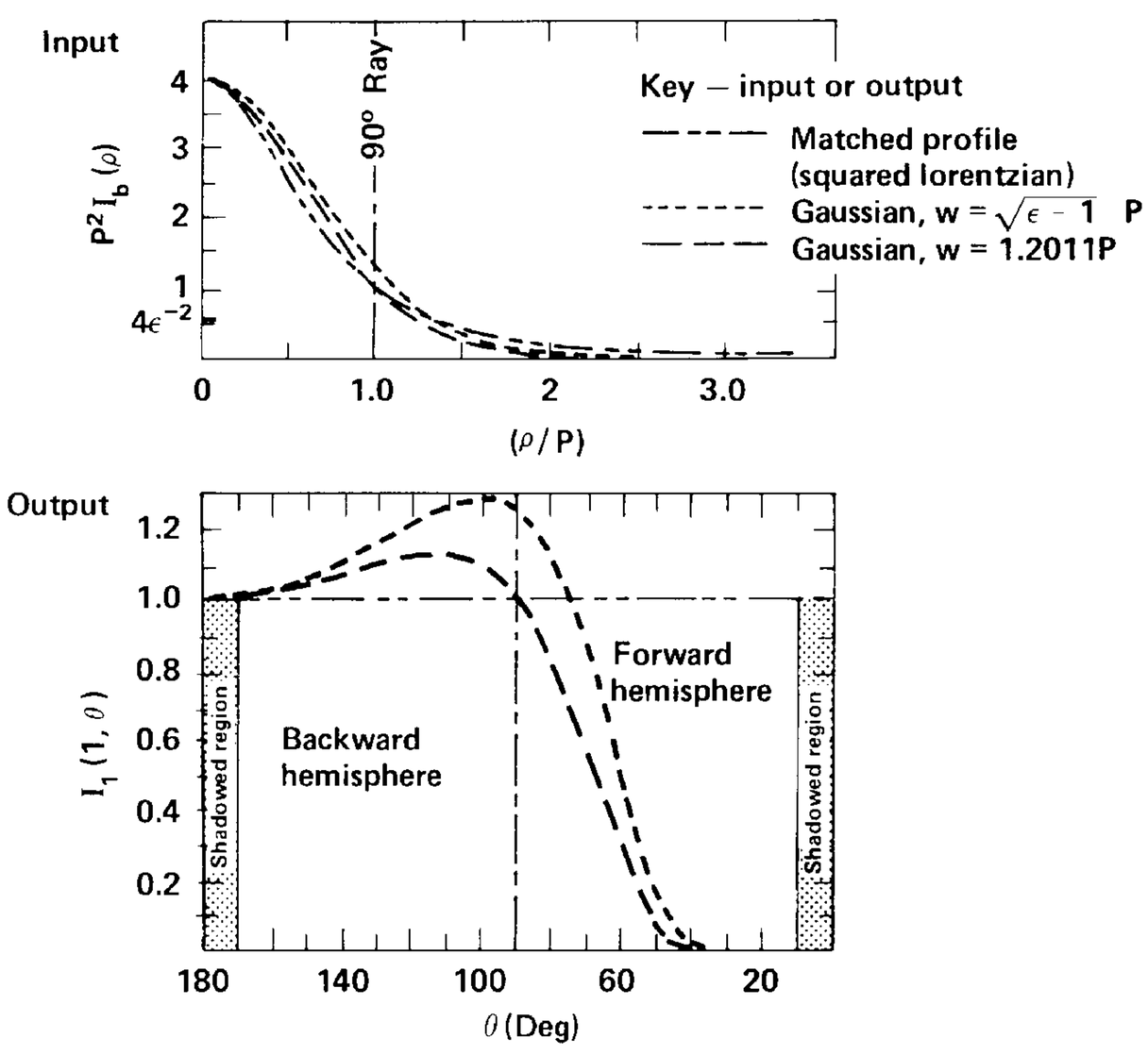

The beam waist w defined as the $1/e^2$ intensity radius of the input distribution given by Eq. (13) is

$$w = (\rho)_{1/e^2} = 2p|(1 - e)/(1 + e)|(\epsilon - 1)^{1/2}. \quad (16)$$

Since $p \ll a$, $w \ll \rho_{\max}$. Figure 2 is a plot of $f(\rho,\theta)$ for $e = 1/3$. Figure 3 is a plot of the output and input intensity distributions for the following functional forms for I_b and $e = 1/3$:

(1) The input distribution given by Eq. (13).

(2) A Gaussian input distribution with beam waist given by Eq. (16).

(3) A Gaussian input with beam waist chosen to give unit intensity in $I_1(1,\theta)$ at 90 and 180 degrees.

From Fig. 3, it can be seen that the output intensity distribution $I_1(1,\theta)$ is critically sensitive to the input beam shape in the forward hemisphere, $0° \leq \theta \leq 90°$, but reasonably insensitive in the backward hemisphere.

The simple system that has been used for preliminary discussions has the added disadvantage of impractical size. The parameter p is determined by damage considerations, while the ratio a/p is determined by the allowable shadow fraction on the target determined by Eq. (15). For example, a 50-J, $e = 1/3$ one-beam system with 2% shadow fraction yields the following design parameters: $w = 2.8$ cm, $p = 2.2$ cm, $a = 205$ cm, assuming a $2 J/cm^2$ mirror flux.

Both these disadvantages are largely alleviated by simply folding the one-beam mirror system, as shown in Fig. 4. Now the eccentricity of the elliptical mirror is fixed at $e = 1/3$. In this way, each elliptical mirror section shares one focus, while the two conjugate foci of each section occur at the surface of the opposite section and are congruent with the virtual foci of two much smaller primaries. This is a more practical system and will be described below.

Fig. 3. Output and input intensity distributions.

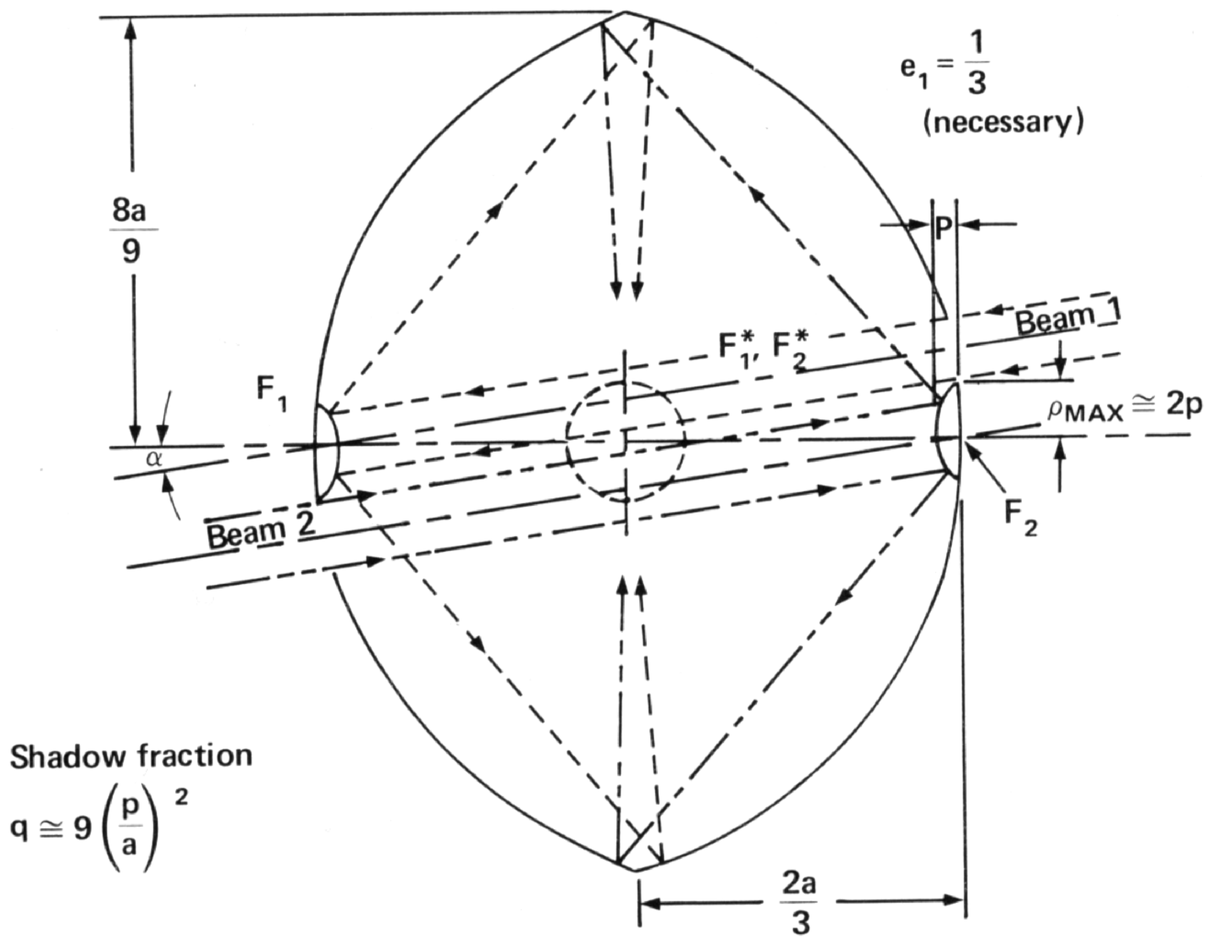

Fig. 4. Two-beam system with tilted parabolic primaries.

Practical Two-beam Illumination Systems

Figures 4 and 5 illustrate two interesting variations of a practical two-beam illumination system. In Fig. 4, synchronous collimated input beams and tilted parabolic primaries are used, while in Fig. 5 the input beams are gently focused on hyperbolic primaries to eliminate that half of the shadowing due to entrance apertures. Otherwise, both schemes have the following advantages in common relative to the single-beam optic:

(1) Only the backward hemisphere ($180° \geq \theta \geq 90°$) distribution is used from each input beam. This greatly reduces sensitivity to input beam shape.

(2) The design involves smaller secondary to primary dimension ratios and thus a smaller overall device for a given shadow fraction.

For hyperbolic primaries, Eqs. (11), (13), (13a), and (16) remain valid for an input lens with focal length equal to the primary optic image distance f, given by

$$f = a(1 + e) - 2p. \tag{17}$$

This equivalence is demonstrated in the Appendix.

The eccentricity of the hyperbolic primaries is not a free parameter, but is required to be

$$e_2 = [(f + p)/(f - p)]. \tag{18}$$

The corresponding input f/number is given by

$$F_{\#} = f/2p. \tag{19}$$

The intersection radius of the two mirror surfaces is

$$\rho_{max} = p(e_2 + 1) \longrightarrow 2p \quad \text{as } e_2 \longrightarrow 1. \tag{20}$$

In this case, $w/\rho_{max} = 0.66$. The shadow fraction is then reduced to

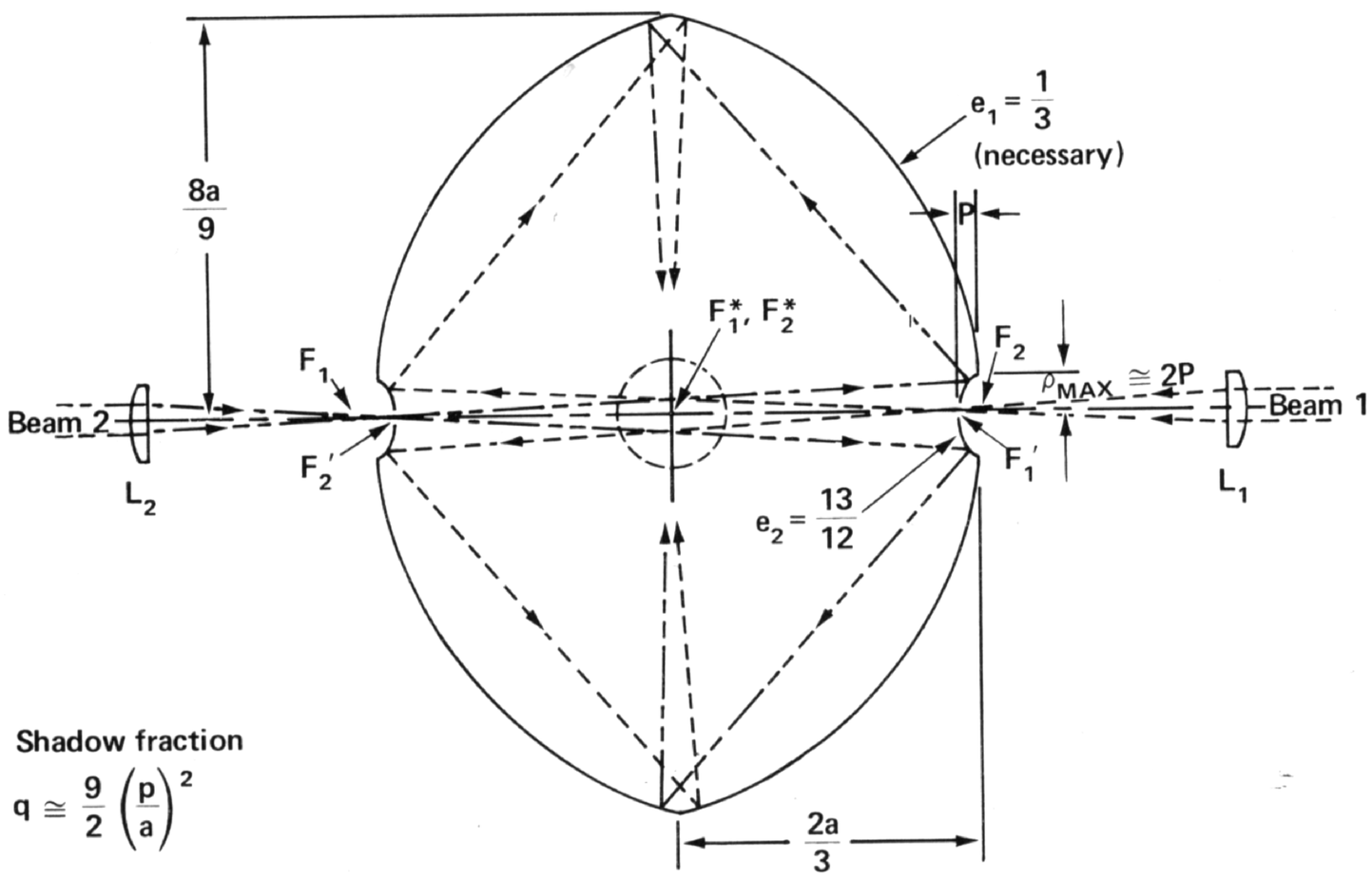

Fig. 5. Two-beam illumination system with on-axis hyperbolic primaries.

$$q = 9(p/a)^2 \quad \text{for parabolic primaries} \tag{21a}$$

and

$$q = (9/2)(p/a)^2 \quad \text{for hyperbolic primaries.} \tag{21b}$$

This last fact is the only special advantage of hyperbolics. Either system has a distinct advantage in size relative to the one-beam system due to the quadratic dependence of q on (p/a). For example, a 50-J mirror system with 2% shadow fraction and 2 J/cm^2 flux limit gives $w = 2.8$ cm, $p = 2.2$ cm, and $a = 47$ cm, with parabolic primaries or $a = 33$ cm with hyperbolics. In the case of the parabolic primary, the required offset angle $\alpha \simeq (9/4)(p/a)$ is about 6°, and the intensity distributions become $f(\rho,\theta \pm \alpha)$. The $F_\#$ of L_1 and L_2 in the system shown in Fig. 5 would be 12.5.

In a practical illumination system intended for fusion research, some provision must be made for diagnostic equipment apertures. If normal incidence on a spherical target is desired, a compromise must be made between illumination coverage and the diagnostic solid angle required. We note, however, that much of the diagnostic solid angle in present laser fusion experimental designs is devoted to optical diagnostics, and that the access needed for this purpose is provided at the entrance pupil of the system described here. X-ray, charged-particle, and neutron detectors, for example, would require some deletion of secondary reflector area. However, illumination systems using multiple discrete optics face this problem as well.

If complete target coverage is required, but precisely normal illumination is not, judicious defocusing is a workable solution for either single or multiple optic illumination devices.

Incidence Angles

In designing practical two-beam illumination systems, it is often useful to compute the ray incidence angles at the primary and secondary reflective surfaces. This is particularly true if multilayer dielectric coatings are to be employed.

In the geometric optics limit, the incidence angle at a spherical target surface is always zero. The angle of incidence on the secondary reflector is $\gamma/2$, where

$$\gamma = \pi - (\theta + \phi), \tag{22}$$

and that on the primary reflector is given by (cf. Appendix)

$$\mu = \psi + (\phi/2) = (\phi/2) + 2 \arctan\{[(e_2 - 1)/(e_2 + 1)] \tan(\phi/2)\}. \tag{23}$$

Further, a more convenient relationship between the angles ϕ and θ results from combining Eqs. (5) and (6),

$$\tan(\phi/2) = [(1 - e)/(1 + e)] \times \cot(\theta/2) \longrightarrow \frac{1}{2} \cot(\theta/2) \quad \text{as } e \longrightarrow \frac{1}{3}. \tag{24}$$

Equation (24) may be used to obtain a direct relation between the radial coordinate ρ in the collimated input to all systems described and the target focus incidence angle θ, given by

$$\rho = p \cot(\theta/2). \tag{25}$$

With θ as a parameter, the parameters $\phi/2$, $\gamma/2$, and ρ are plotted in Fig. 6, along with the angle μ for $e_2 = 1.0$ and $e_2 = 13/12$. It is seen that these angles of incidence are never large in practical devices.

Focusing Properties

For definiteness, assume that a Gaussian profile beam is incident on a structure such as shown in Fig. 4 or 5, with divergence m times worse than the diffraction-limited half-angle

$$d\psi = \lambda/\pi w. \tag{26}$$

Conservation of etendue in formation of a focal region with $1/\epsilon^2$ radius r_s implies that

$$r_s = m\lambda/2\pi. \tag{27}$$

A similarly derived estimate of the focal radius attainable with a sharply apertured input beam of uniform intensity gives

$$r_s = 0.40m\lambda. \tag{28}$$

Exact calculation of the focal intensity distribution must include the effects of input beam apodization and divergence due to sources other than diffraction, as well as manufacturing tolerances, and is not attempted here. In fact, geometrical optics will dominate propagation to the critical density surface of laser fusion targets throughout the irradiation sequence, since such targets are typically of the order 100 incident wavelengths in diameter.

Therefore, the preceding estimates indicate that a well-made spherical illumination structure of the type described is quite tolerant to input beam wavefront distortion in the laser fusion application.

Summary

Reflective optics employing various conic sections have been shown to give nearly uniform illumination

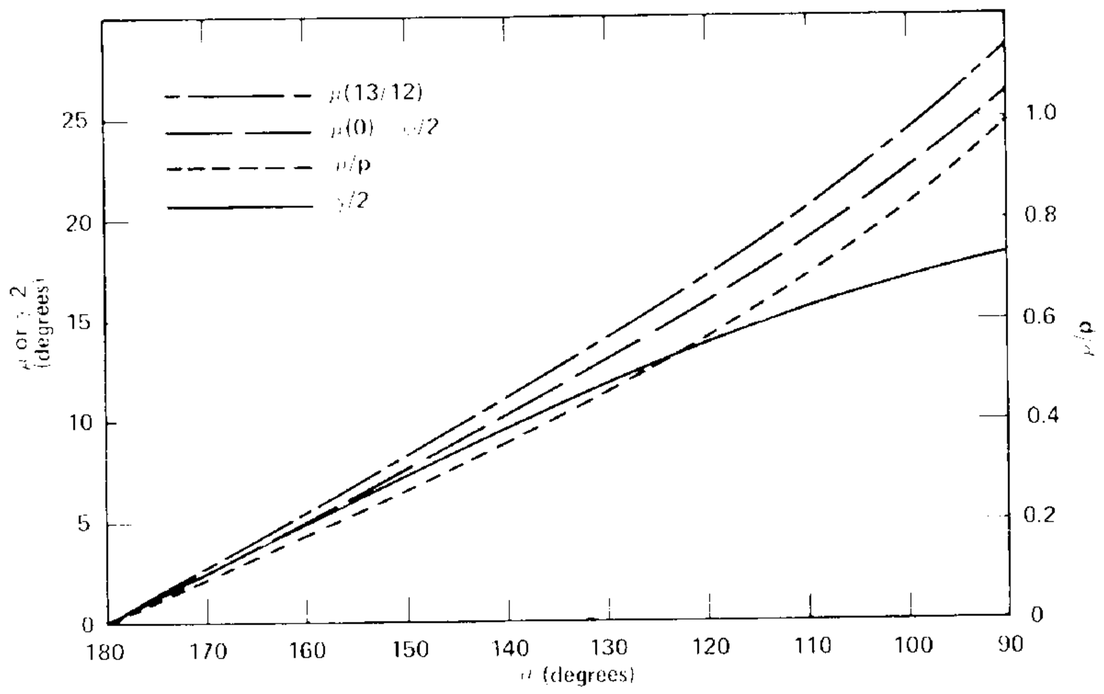

Fig. 6. Dependent of ϕ, ρ, γ, and μ in θ in a two-beam illumination system.

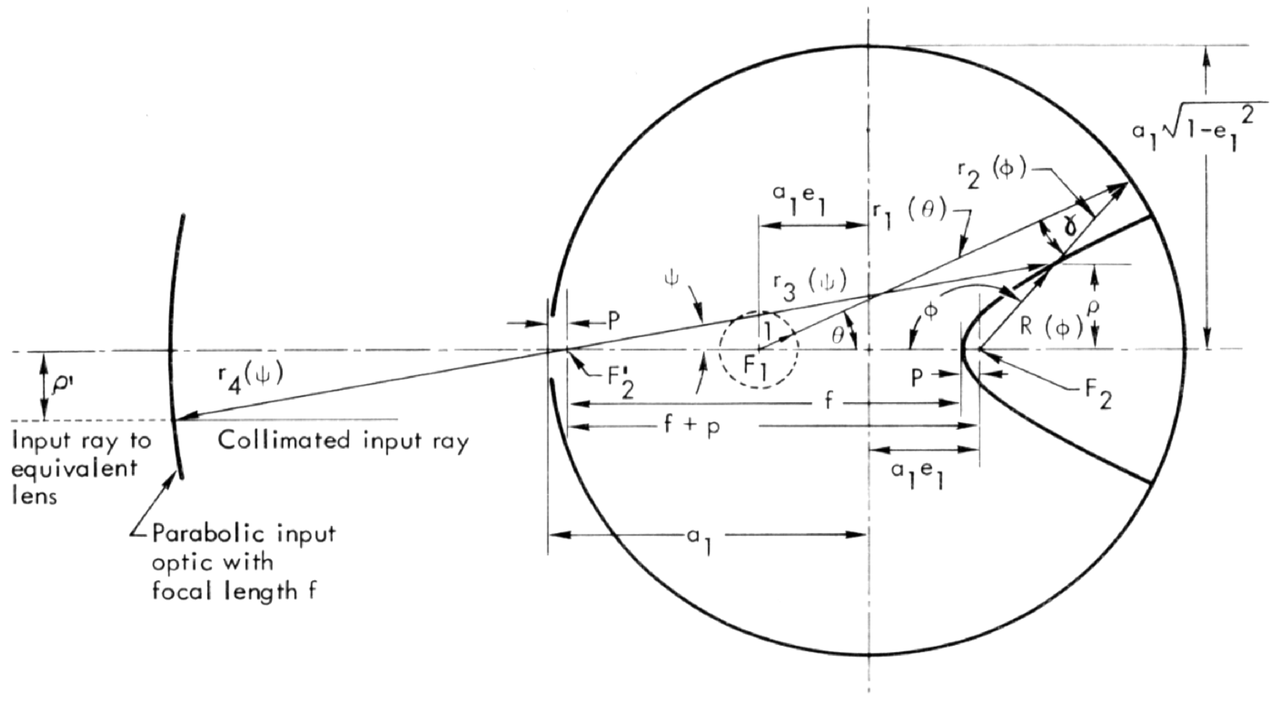

Fig. 7. One-beam illumination system with hyperbolic primary and parabolic input reflector.

of a sphere with one or two laser beams. Two-beam optics yield mirror systems of practical size for early pellet irradiation experiments.

Acknowledgment

The authors were stimulated to begin this design work after learning that KMS Industries, Inc. had developed some type of elliptic mirror system for pellet irradiation.

This work was performed under the auspices of the United States Atomic Energy Commission.

Appendix: Irradiation Systems with Hyperbolic Primary Optics

In the section on two-beam irradiation systems, it was implied that the intensity mapping properties of such devices are independent of the primary optic image distance. Finite image distance is obtained with a hyperbolic primary reflector and is useful to minimize shadowing of the target region due to the irradiation system input aperture as well as to permit collimation of light reradiated by the target plasma. In this section, it will be shown that the analysis developed for a parabolic primary (infinite image distance) is unchanged by substitution of a system consisting of a hyperbolic primary (finite image distance f) combined with an external input optic with focal length f.

Such a system is illustrated in Fig. 7. For clarity, this approach will be illustrated in a one-beam geometry as in Fig. 1. In the figure, an elliptical mirror of eccentricity e_1 and semimajor axis a_1 has the target pellet at the focus labeled F_1. A convex hyperbolic mirror with virtual image distance p and eccentricity $e_2 \geq 1$ shares the major axis and conjugate focus F_2 of the elliptic mirror. A cylindrically symmetric, collimated input beam has radial intensity distribution $I_b(\rho')$ and shares the elliptic mirror major axis. Input radiation is focused on the real image point (F_2') of the primary optic by an external input optic that is equivalent to a parabola with focal length f. From the virtual focus at F_2 to the target, this system is identical to that shown in Fig. 1.

In this case, the hyperbolic mirror surface is given by

$$R(\phi) = [\,p(e_2 + 1)/(1 + e_2 \cos\phi)]. \quad \text{(A1)}$$

The elliptical mirror surface is given by Eq. (3) of the text, and the relationships given by Eqs. (5) through (8) still apply. New parameters are r_4, the distance from the equivalent input optic surface to F_2'; r_3, the distance from F_2' to the point of reflection on the hyperbola; and ψ, which is the cone half-angle of that ray which enters the system at radius ρ' in the collimated input beam.

As stated in Eq. (18), e_2 is not a free parameter, but is chosen so as to place the real image point F_2' a distance p inside the elliptical surface. An alternate form of Eq. 18 that is more useful here is

$$f/p = [(e_2 + 1)/(e_2 - 1)]. \quad \text{(A2)}$$

By analogy with Eq. (2), the equivalent input mirror surface is given by

$$r_4(\psi) = f \sec^2(\psi/2). \quad \text{(A3)}$$

The input ray radius ρ' is related to r_4 and ψ by

$$\rho'(\psi) = r_4 \sin\psi = 2p[(e_2 + 1)/(e_2 - 1)] \tan(\psi/2). \quad \text{(A4)}$$

From the properties of a hyperbola, the parameters r_3 and R are related by the expression

$$r_3(\psi) = R(\phi) + [2p/(e_2 - 1)]. \quad \text{(A5)}$$

In this problem, the forward transfer function is given by

$$f(\rho', \theta) = I_1(1, \theta)/I_b(\rho') = (Rr_1r_4/r_2r_3)^2 = [g(\rho', \theta)]^{-1}. \quad \text{(A6)}$$

Since (r_1/r_2) is completely determined by the secondary elliptical optic that is unchanged from that discussed in the text, equivalence will have been demonstrated between the mapping functions for devices with parabolic and hyperbolic primary systems if it can be shown that

$$(Rr_4/r_3) \stackrel{?}{=} R_p = p \sec^2(\phi/2), \quad \text{(A7)}$$

where R_p is the parabolic primary surface given by Eq. (2) of the text and R is the hyperbolic surface [cf. Eq. (A1)]. This statement is clear upon comparing the mapping function forms for the two cases [cf. Eqs. (10) and (A6)]. The proof of Eq. (A7) proceeds as follows. By inspection of Fig. 7 together with Eqs. (A1), (A2), and (A5),

$$\cos\psi = \{|(f + p) - R\cos\phi|/r_3\}$$

$$= \left\{\frac{|2pe_2/(e_2 - 1)| - R\cos\phi}{|2p/(e_2 - 1)| + R}\right\}$$

$$= \left[\frac{2e_2 + (e_2^2 + 1)\cos\phi}{2e_2\cos\phi + (e_2^2 + 1)}\right]. \quad \text{(A8)}$$

Therefore,

$$\tan^2(\psi/2) = |(1 - \cos\psi)/(1 + \cos\psi)|$$

$$= |(e_2 - 1)/(e_2 + 1)|^2|(1 - \cos\phi)/(1 + \cos\phi)|$$

and

$$\tan(\psi/2) = |(e_2 - 1)/(e_2 + 1)|\tan(\phi/2). \quad \text{(A9)}$$

Now,

$$\rho'/\rho = r_4\sin\psi/r_3\sin\psi = r_4/r_3, \quad \text{(A10)}$$

where, as before,

$$\rho = R\sin\phi. \quad \text{(A11)}$$

By combining Eqs. (A4) and (A9), we find that

$$\rho' = 2p\tan(\phi/2). \quad \text{(A12)}$$

It follows from Eqs. (A10), (A11), and (A12) that

$$(Rr_4/r_3) = (R\rho'/\rho) = p\sec^2(\phi/2) \quad \text{(A7)}$$

as was to be proved.

Therefore, Eqs. (11), (13), (13a), (16), and (25) of the text remain valid for a system employing a hyperbolic primary with finite image distance f combined with an external input optic with focal length f when the radial coordinate is relabeled ρ'.

Two additional differential relationships analogous to Eqs. (8) and (9) appear in this system. Differentiation of Eq. (A4) together with Eq. (A2) gives

$$d\rho' = p|(e_2 + 1)/(e_2 - 1)|\sec^2(\psi/2)d\psi = r_4(\psi)d\psi. \quad \text{(A13)}$$

Also, Eq. (A9) may be differentiated and combined with Eqs. (A2) and (A13) to give

$$r_4(\psi)d\psi = p\sec^2(\phi/2)d\phi.$$

This expression may be combined with Eqs. (A10) through (A12) to give

$$r_3(\psi)d\psi = (\rho/\rho')r_4d\psi = R[r_4d\psi/p\sec^2(\phi/2)] = R(\phi)d\phi. \quad \text{(A14)}$$

References

1. J. Nuckolls, J. Emmett, and L. Wood, Phys. Today **26**, 46 (August 1973).
2. J. Nuckolls, L. Wood, A. Thiessen, and G. Zimmerman, Nature **239**, 139 (1972).
3. M. Born and E. Wolf, *Principles of Optics* (Pergamon Press, Oxford, 1965).
4. General approaches for calculating the optical transfer properties of more complex reflective geometries are contained in G. Minerbo, *Los Alamos Scienific Laboratory Report* LA-UR 74-604 and J. H. McDermit and T. E. Horton, Appl. Opt. **13**, 1444 (1974).